Preprints (www.preprints.org) | NOT PEER-REVIEWED | Posted: 11 October 2019 doi:10.20944/preprints201910.0121.v1

Peer-reviewed version available at Pathogens 2019, 8, 240; doi:10.3390/pathogens8040240

Article

Electrocardiography Abnormalities in Macaques after Infection with Encephalitic Alphaviruses

Henry Ma[1], Jeneveve D. Lundy[1], Katherine J. O'Malley[1], William B. Klimstra[1,*], Amy L. Hartman[1,*], and Douglas S. Reed[1,*]

[1] Center for Vaccine Research, University of Pittsburgh, Pittsburgh, PA, USA
* Correspondence: dsreed@pitt.edu

Abstract: Eastern (EEEV) and Venezuelan (VEEV) equine encephalitis viruses (EEVs) are related, (+)ssRNA arboviruses that can cause severe, sometimes fatal, encephalitis in humans. EEVs are highly infectious when aerosolized, raising concerns for potential use as biological weapons. No licensed medical countermeasures exist; given the severity/rarity of natural EEV infections, efficacy studies require animal models. Cynomolgus macaques exposed to EEV aerosols develop fever, encephalitis, and other clinical signs similar to humans. Fever is nonspecific for encephalitis in macaques. Electrocardiography (ECG) metrics may predict onset, severity, or outcome of EEV-attributable disease. Macaques were implanted with thermometry/ECG radiotransmitters and exposed to aerosolized EEV. Data was collected continuously, and repeated-measures ANOVA and frequency-spectrum analyses identified differences between courses of illness and between pre-exposure and post-exposure states. EEEV-infected macaques manifested widened QRS-intervals in severely ill subjects post-exposure. Moreover, QT-intervals and RR-intervals decreased during the febrile period. VEEV-infected macaques suffered decreased QT-intervals and RR-intervals with fever onset. Frequency-spectrum analyses revealed differences in the fundamental frequencies of multiple metrics in the post-exposure and febrile periods compared to baseline and confirmed circadian dysfunction. Heart rate variability (HRV) analyses revealed diminished variability post-exposure. These analyses support using ECG data alongside fever and clinical laboratory findings for evaluating medical countermeasure efficacy.

Keywords: alphavirus; vaccine; arbovirus; animal models; nonhuman primates; electrocardiography; ECG; aerosol; encephalitis; equine

1. Introduction

Equine encephalitis viruses (EEVs) constitute a distinct portion of the alphavirus genus of Family *Togaviridae*. Alphaviruses are grouped into New World and Old World viruses, which generally correspond with signs of clinical disease; New World alphaviruses are more likely to cause encephalitis while Old World viruses tend to cause arthralgia [1-4]. These mosquito-borne viruses were the first alphaviruses to be isolated through the 1930s, and VEEV underwent research in later decades by the United States and the Union of Soviet Socialist Republics as a potential biological warfare agent after it was realized that VEEV was highly infectious when aerosolized [5-10]. These pathogens remain important medical and veterinary pathogens to this day [11].

In the clinical context, encephalitis comprises infection or inflammation of brain parenchyma that may produce signs of diagnosable disease [12]. EEVs can produce a febrile course, the eponymous encephalitis, and a variety of neurological presentations including but not limited to seizures, tremor, and photophobia [1,12]. Other symptoms seen in EEV-induced disease includes nausea, vomiting, diarrhea, focal neurological deficits, or altered mental status [13-18]. VEEV and western equine encephalitis virus are only rarely fatal in naturally-transmitted human cases, and

© 2019 by the author(s). Distributed under a Creative Commons CC BY license.

Preprints (www.preprints.org) | NOT PEER-REVIEWED | Posted: 11 October 2019 doi:10.20944/preprints201910.0121.v1

Peer-reviewed version available at Pathogens 2019, 8, 240; doi:10.3390/pathogens8040240

then typically only in very young or elderly patients [15,19-24]. North American isolates of EEEV have a high case fatality rate, estimated to range from 30-70%, although sub-clinical disease may be underreported [13,25]. Survivors of virulent infections can develop persistent neurologic sequelae that affect motor function. Pathological evaluation can confirm or rule out encephalitis by examination of cellular inclusion bodies, lymphocytic infiltrates, and immunohistochemical staining; however, the post-mortem nature of these procedures limits their clinical applicability [26]. Apart from a thorough patient history, confirmation of EEVs as the cause of disease requires detection of EEV-specific IgM or IgG in plasma or cerebrospinal fluid (CSF) [13,18,27].

No consensus governs the case management of EEV infections and no licensed treatments or vaccines are available to mitigate an outbreak or intentional release [1,28]. Because aerosol dissemination is not a natural route of transmission, determining efficacy of countermeasures against aerosolized EEVs in a clinical trial is neither logistically nor ethically possible. Licensure of such countermeasures can proceed only through the FDA's Animal Rule, which allows for pivotal efficacy studies to be conducted in well-characterized animal models that meet appropriate criteria [29]. These criteria require that the disease and pathophysiology in the animal model must resemble what is known to occur in humans. To evaluate the efficacy of a therapeutic treatment against viral encephalitis, biomarkers that correspond with viral penetration into the CNS and/or neurological disease severity are needed. For EEVs, infection of the cynomolgus macaque closely resembles the disease seen in humans [30,31]. Fever was the predominant physiological sign observed in past EEV studies, but it is not clear if this corresponds with a response to peripheral viral replication or viral penetration into the CNS [18,32-34]. In VEEV infection of humans and macaques, the febrile response is biphasic; the consensus in the field has been that the first fever likely represents peripheral viral replication while the second fever coincides with viral penetration into the CNS. In macaques, the second febrile period is associated with neurological signs indicative of encephalitis [35]. In contrast, EEEV infections do not have a fever in the initial period seen with VEEV but fever onset roughly corresponds with the second fever peak for VEEV and onset of neurological signs in macaques [36]. Previous work with macaques found that heart rate increased in association with fever onset after infection with EEEV [35,36]. Exploration of a wider range of electrocardiographic metrics leverages the advantages inherent in continuous radiofrequency telemetry monitoring equipment. In this study, we hypothesized that physiological changes encountered in macaques following infection with EEEV or VEEV would produce measurable changes in electrocardiographic metrics that would precede or accompany the onset of febrile or encephalitic disease. We performed repeated measures ANOVA and multiple comparisons of electrocardiographic metrics between pre-exposure, post-exposure, febrile periods for macaques that developed fever, and recovery periods for macaques that survived febrile courses. Heart rate variability (HRV) was analyzed between days from the baseline period through the post-infection period. Finally, frequency-spectrum analysis was performed on the electrocardiography metrics. Findings indicated that changes in QRS complexes, QT-Interval, and RR-Interval, among other metrics, could serve as sentinels of EEV-induced disease.

2. Results

2.1. ECG Changes in EEEV-infection of Macaques

To explore the utility of monitoring ECG changes associated with EEEV-induced viral encephalitis caused by New World-alphaviruses, four macaques were exposed to small-particle (≤5μm mass mean aerodynamic diameter) aerosols containing EEEV. The outcome and the febrile response after infection of the macaques with EEEV are shown in Table 1. Macaques exposed to EEEV manifested either severe or non-severe courses of disease (Figure 1a). Severe disease was defined as a course that precipitated moribund status requiring euthanasia. Aerosol exposure to EEEV produced severe disease courses in the two macaques (M161-16, M163-16) that received more than $1.1*10^8$ PFU. In contrast, the two macaques (M160-16, M162-16) that received doses below this amount survived without fever.

Preprints (www.preprints.org) | NOT PEER-REVIEWED | Posted: 11 October 2019 doi:10.20944/preprints201910.0121.v1

Peer-reviewed version available at Pathogens 2019, 8, 240; doi:10.3390/pathogens8040240

Table 1. EEV Courses of Infection in Macaque Cohort. Macaques received aerosols of either EEEV or VEEV. *Doses in log_{10} pfu. £Neuro = neurological signs (tremors, seizures, photophobia, head pressing), δTTD = Time to death, S = Survived to 28 days post infection. ɣFever data. ΔMax = maximum difference from predicted; Onset = onset of fever duration > 8 hrs; Duration = fever duration, in hours; Fever-hours = summation of all significant differences in temperature from predicted.

Virus	Macaque	Sex	Dose*	TTDδ	Neuro£	ΔMaxɣ	Onsetɣ	Durationɣ	Fever-hoursɣ
EEEV	161-16	M	8.2	6	Y	4.2	3	70.8	144.2
	163-16	M	7.5	6	Y	4.4	3	65.0	154.9
	Mean					**4.3**	**3**	**67.9**	**149.6**
	160-16	M	7.0	S	N	0.7		14.3	6.5
	162-16	M	5.7	S	N	1.8		41.5	30.5
	Mean					**1.3**		**27.9**	**18.5**
VEEV	164-16	F	7.1	S	Y	2.8	1	187.8	171.6
	165-16	F	6.9	S	Y	3.1	1	260.5	282.5
	170-16	M	6.3	S	Y	2.9	1	180.5	153.8
	171-16	M	6.0	S	Y	3.3	1	238.0	305.9
	Mean					**3.0**	**1**	**216.7**	**228.4**

In the macaques with severe EEEV disease (M161-16, M163-16), the disease course replicated with high fidelity what was reported previously with a different EEEV strain [36]. Post-challenge, the macaques became febrile shortly after the 3-day mark, culminating in a febrile plateau of 40-41°C around 4.0 days post-infection (dpi) (Figure 1b,c). This plateau was followed by a terminal decline in temperature beginning approximately 5 dpi, heralding a moribund state occurring at approximately 6 dpi. For macaques with severe disease, 0-3 dpi defined the post-infection period and the time following 3 dpi denoted the febrile period. None of the EEEV-infected macaques with severe disease survived, so a recovery period was not defined. For the two macaques that survived lower doses of EEEV there was no febrile response post-infection (Figure 1d,e) nor any changes in behavior or activity or any other clinically apparent sequelae.

In the immediate post-infection period, the profile of QRS Complex data show no readily apparent changes between 0 dpi to 3 dpi, in either the directly observable trace (Figure 2a) or in daily aggregates of the QRS complex (Figure 2b). Beginning with fever onset on 3 dpi, the QRS complex exhibited progressive increases in severely diseased EEEV-infected macaques which continued until euthanasia criteria were met (Table 2, $p<0.05$). Macaques exposed to the lower doses of EEEV displayed no significant deviations from their baseline QRS complexes (Figure 2b).

Similar to the QRS-Interval, there are no visually apparent changes for any of the EEEV-infected macaques in the QT-interval trace (Figure 3a) or the daily QT-interval aggregate (Figure 3b) in the post-infection period until 3 dpi. With the onset of fever on 3 dpi, the two macaques with severe EEEV disease exhibited shortened QT-intervals and a loss of diurnal variation. This continued until the macaques were moribund (Table 3, $p<0.05$). A false positive result surfaced from the repeated measures ANOVA for M160-16, one of the macaques without severe disease, but this result is attributable to data loss during baseline collection; (Figure 3a) this effect disappears once the days containing missing baseline data are censored. The missing diurnal baseline data for 160-16 rendered an apparent increase in QT-interval on the initial analysis. In the macaques exposed to

Preprints (www.preprints.org) | NOT PEER-REVIEWED | Posted: 11 October 2019 doi:10.20944/preprints201910.0121.v1

Peer-reviewed version available at Pathogens 2019, 8, 240; doi:10.3390/pathogens8040240

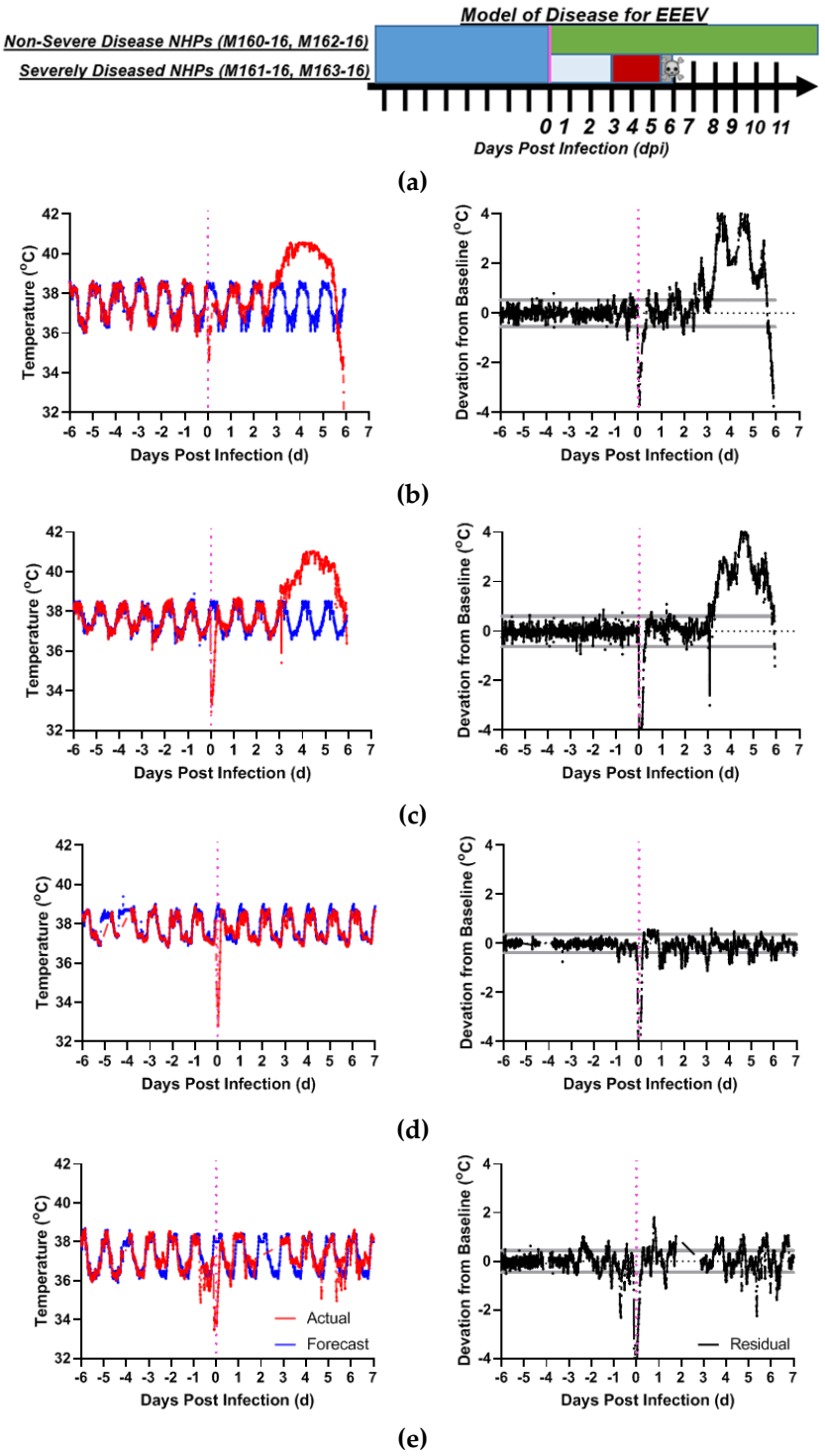

Figure 1. EEEV disease in macaques. Shown are models of disease for **(a)** EEEV-exposed macaques with non-severe and severe courses of alphavirus disease over days post-infection (x-axis). Deep blue denotes pre-infection baseline period, vertical magenta line denotes time of infection. Green bar denotes post-infection period in animals without severe/fatal disease. For animals with severe/fatal disease, powder blue defines post-infection period before the onset of fever, and red signifies the febrile post-infection period. Skull and crossbones mark the mean time to death. Actual and forecasted temperature profiles for two macaques with severe disease requiring euthanasia: **(b)** M161-16, and **(c)** M163-16, compared to macaques without severe disease: **(d)** M160-16 and **(e)** M162-16. Red: Actual Temperature (°C), Blue: Forecasted Temperature (°C) from ARIMA modeling, Black: Residual Values (°C) (deviations from forecasted baseline). Gray Lines: upper/lower bounds for residuals Magenta: aerosol challenge.

Preprints (www.preprints.org) | NOT PEER-REVIEWED | Posted: 11 October 2019 doi:10.20944/preprints201910.0121.v1

Peer-reviewed version available at Pathogens 2019, 8, 240; doi:10.3390/pathogens8040240

lower doses of EEEV that did not develop clinical disease, no reductions or loss of diurnal variation in QT-Interval were seen in the study period (Figure 3b).

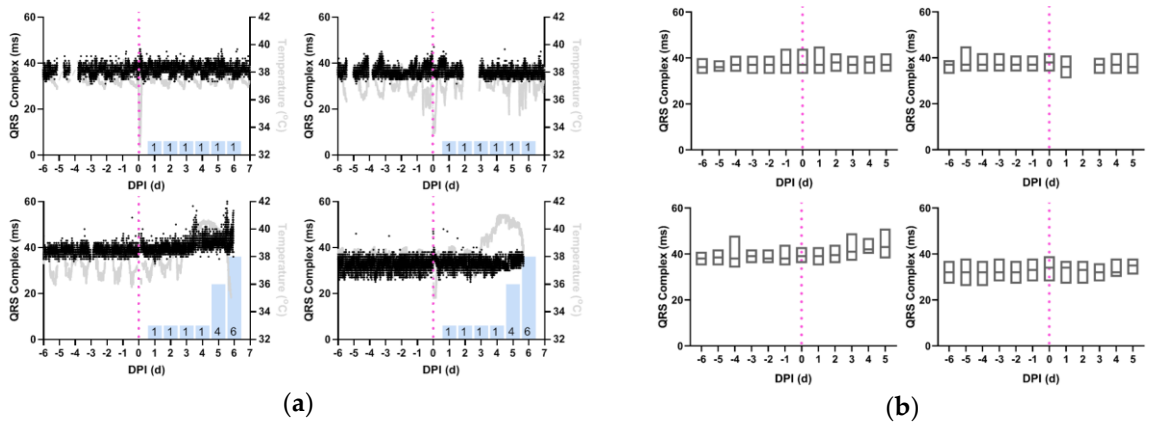

(a) (b)

Figure 2. Increase in QRS Complex during the febrile period in macaques with severe EEEV. Shown are the profiles **(a)** of QRS complex derived from 1-minute average measurements for four individual macaques infected with EEEV. Black: QRS Complex (ms), Gray: Temperature (°C), and Magenta: aerosol challenge. Blue Bars: Neurological score on corresponding day. **(b)** Average daily QRS Complex measurements, from repeated measures ANOVA, depicted in with boxes delimited by interquartile range and center line signifying median value. For **(a)** and **(b)**, Top Left: M160-16, Bottom Left: M161-16, Top Right: M162-16, Bottom Right: M163-16.

Table 2. Repeated Measures ANOVA Statistics for QRS Complexes. Statistics and p-values for QRS complex for EEEV and VEEV-infected macaque cohorts. [£]Doses in $\log_{10}$ pfu. [δ]TTD = Time to death. *P-Value lower than significance level α=0.05.

Virus	Macaque	Sex	Dose[£]	TTD[δ]	F-Statistic	P-Value
EEEV	M161-16	M	8.2	6	4.780	0.0346*
	M163-16	M	7.5	6	4.034	0.0490*
	M160-16	M	7.0	S	3.833	0.058
	M162-16	M	5.7	S	3.046	0.331
VEEV	M164-16	F	7.1	S	29.55	<0.00001*
	M165-16	F	6.9	S	164.7	<0.00001*
	M170-16	M	6.3	S	48.40	<0.00001*
	M171-16	M	6.0	S	84.17	<0.00001*

RR-intervals in macaques infected with EEEV follow a similar pattern to that seen with the QT-Interval (Figure 4a). From challenge to 3 dpi, there was no visual change in RR-Interval in any of the macaque. On 3 dpi, the severely-infected macaques had decreases in both the trace and the median RR-interval in aggregate data (Figure 4b). No changes in RR-Interval were observed for macaques with nonsevere courses of disease (Table 4, $p<0.05$).

Heart rate variability was plotted as ordered pairs of the RR-interval data collected at time n (RRI_n) and RR-interval data collected at time $n+1$ (RRI_{n+1}), wherein n represents an integer value in corresponding to a minute on the macaque's time scale. In aggregate, when these scatter plots are superimposed and color-coded by pre-infection, post-infection, and febrile disease periods (Figure 5a), there is a visually notable contraction in the distribution of ordered pairs during the febrile period in the severely diseased macaques. When decomposed into Poincaré plots to showcase the day to day distribution of heart rate variability, with the central tendency of the plots represented by the geometric mean (Supplemental Figures A1 and A2), the disease courses of the severely diseased macaques demonstrate (Figure 5b) a statistically significant decrease in the geometric mean of the

Preprints (www.preprints.org) | NOT PEER-REVIEWED | Posted: 11 October 2019 doi:10.20944/preprints201910.0121.v1

Peer-reviewed version available at Pathogens 2019, 8, 240; doi:10.3390/pathogens8040240

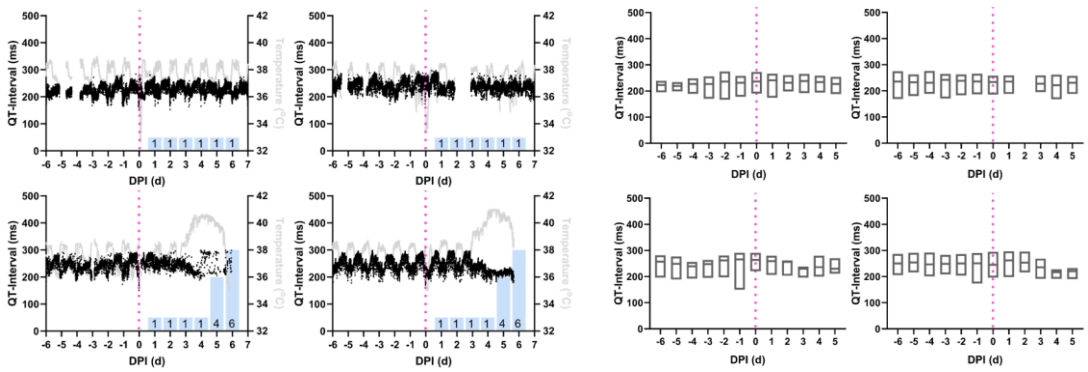

(a) (b)

Figure 3. Reduction in QT-Interval during the febrile period in macaques infected with severe EEEV. Shown are the profiles **(a)** of QT-Interval derived from 1-minute average measurements for four individual macaques infected with EEEV. Black: QT-Interval (ms), Gray: Temperature (°C), and Magenta: aerosol challenge. Blue Bars: Neurological score on corresponding day. **(b)** Average daily QT-Interval measurements, from repeated measures ANOVA, depicted in with boxes delimited by interquartile range and center line signifying median value. For **(a)** and **(b)**, Top Left: M160-16, Bottom Left: M161-16, Top Right: M162-16, Bottom Right: M163-16.

Table 3. Repeated Measures ANOVA Statistics for QT-Interval. Statistics and p-values for QT-interval for EEEV and VEEV-infected macaque cohorts. [£]Doses in $\log_{10}$ pfu. [δ]TTD = Time to death. *P-Value lower than significance level α=0.05.

Virus	Macaque	Sex	Dose*	TTD[δ]	F-Statistic	P-Value
EEEV	M161-16	M	8.2	6	6.472	0.016*
	M163-16	M	7.5	6	24.95	0.00005*
	M160-16	M	7.0	S	3.884	0.055
	M162-16	M	5.7	S	2.962	0.335
VEEV	M164-16	F	7.1	S	36.30	<0.00001*
	M165-16	F	6.9	S	62.56	<0.00001*
	M170-16	M	6.3	S	25.46	<0.00001*
	M171-16	M	6.0	S	82.35	<0.00001*

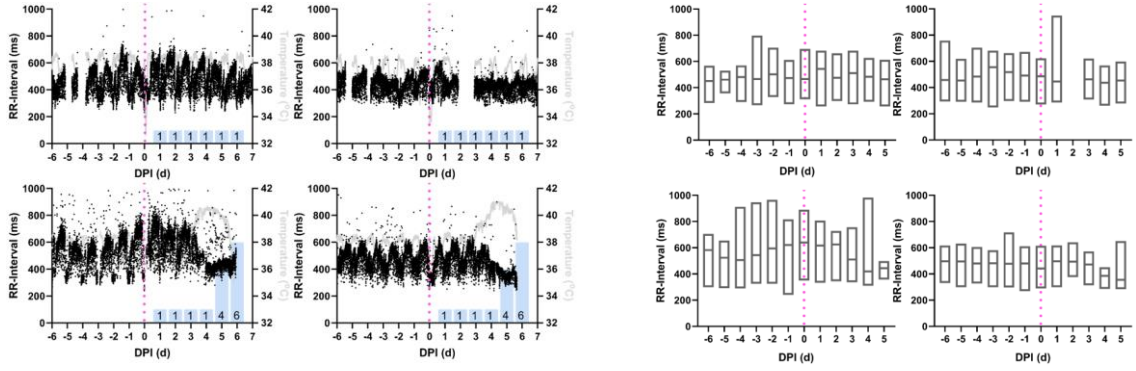

(a) (b)

Figure 4. Reduction in RR-Interval during the febrile period in macaques infected with EEEV. Shown are the profiles **(a)** of RR-Interval derived from 1-minute average measurements for four individual macaques infected with EEEV. Black: RR-Interval (ms), Gray: Temperature (°C), and Magenta: aerosol challenge. Blue Bars: Neurological score on corresponding day. **(b)** Average daily RR-Interval measurements, from repeated measures ANOVA, depicted in with boxes delimited by interquartile range and center line signifying median value. For **(a)** and **(b)**, Top Left: M160-16, Bottom Left: M161-16, Top Right: M162-16, Bottom Right: M163-16.

Preprints (www.preprints.org) | NOT PEER-REVIEWED | Posted: 11 October 2019 doi:10.20944/preprints201910.0121.v1

Peer-reviewed version available at Pathogens 2019, 8, 240; doi:10.3390/pathogens8040240

distribution ($p<0.05$) with an accompanying diminishment of variability, which recapitulates the markedly reduced heart rate variability roughly corresponding to the results seen in Figure 4.

Table 4. Repeated Measures ANOVA Statistics for RR-Interval. Statistics and p-values for RR-Interval for EEEV and VEEV-infected macaque cohorts. [£]Doses in log_{10} pfu. [δ]TTD = Time to death. *P-Value lower than significance level α=0.05.

Virus	Macaque	Sex	Dose*	TTD[δ]	F-Statistic	P-Value
EEEV	M161-16	M	8.2	6	6.626	0.014*
	M163-16	M	7.5	6	13.92	0.0004*
	M160-16	M	7.0	S	3.420	0.073
	M162-16	M	5.7	S	2.227	0.376
VEEV	M164-16	F	7.1	S	49.07	<0.00001*
	M165-16	F	6.9	S	175.9	<0.00001*
	M170-16	M	6.3	S	15.65	<0.00001*
	M171-16	M	6.0	S	183.0	<0.00001*

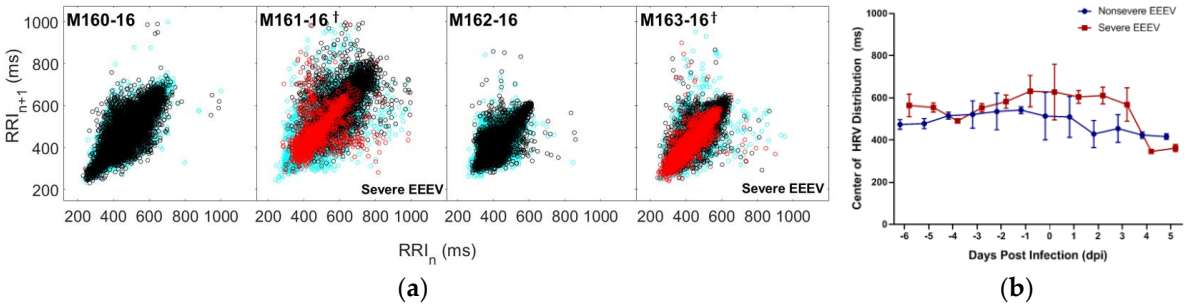

(a) (b)

Figure 5. Heart Rate Variability decreases during the febrile period in macaques infected with EEEV. (a) Distributions of heart rate variability of each EEEV-infected macaque are plotted in aggregate EEEV and color-coded by disease period (Cyan: Pre-Infection, Black: Post-Infection, Red: Febrile (if applicable)). **(b)** Repeated measures ANOVA of HRV data for macaques with nonsevere and severe EEEV infection ($p<0.05$). Central tendency of macaques with severe disease (Red) significantly diminishes after 3 dpi, compared to macaques with nonsevere disease (Blue).

2.2. ECG Changes in VEEV-infection of Macaques

Aerosol parameters of VEEV-infected macaques are summarized in Table 1. Exposure to VEEV produced a characteristic biphasic febrile illness in all exposed macaques with the first phase beginning within 18-24 hours post-infection and the second phase within 1-3 days after the first phase had resolved (Figure 6a). None of the macaques challenged with VEEV died from the disease, and all recovered from their fevers. Post-exposure, macaques became febrile after a latency period of a day, with a febrile peak of 40-41°C at approximately 1.3 dpi (Figure 6b-e). The temperature returned to normal by 1.5 dpi. A second fever occurred at 2.5 dpi and lasted approximately four days until 6.5-7.0 dpi. Subsequently, the macaques' temperatures returned to normal, with the exception of hypothermia that occurred in M165-16. For analysis of VEEV-infected macaques, the post-infection period was defined as 0-1 dpi (inclusive), the febrile period as 2-7 dpi (inclusive), and the recovery period as 8+ dpi.

Preprints (www.preprints.org) | NOT PEER-REVIEWED | Posted: 11 October 2019 doi:10.20944/preprints201910.0121.v1

Peer-reviewed version available at Pathogens 2019, 8, 240; doi:10.3390/pathogens8040240

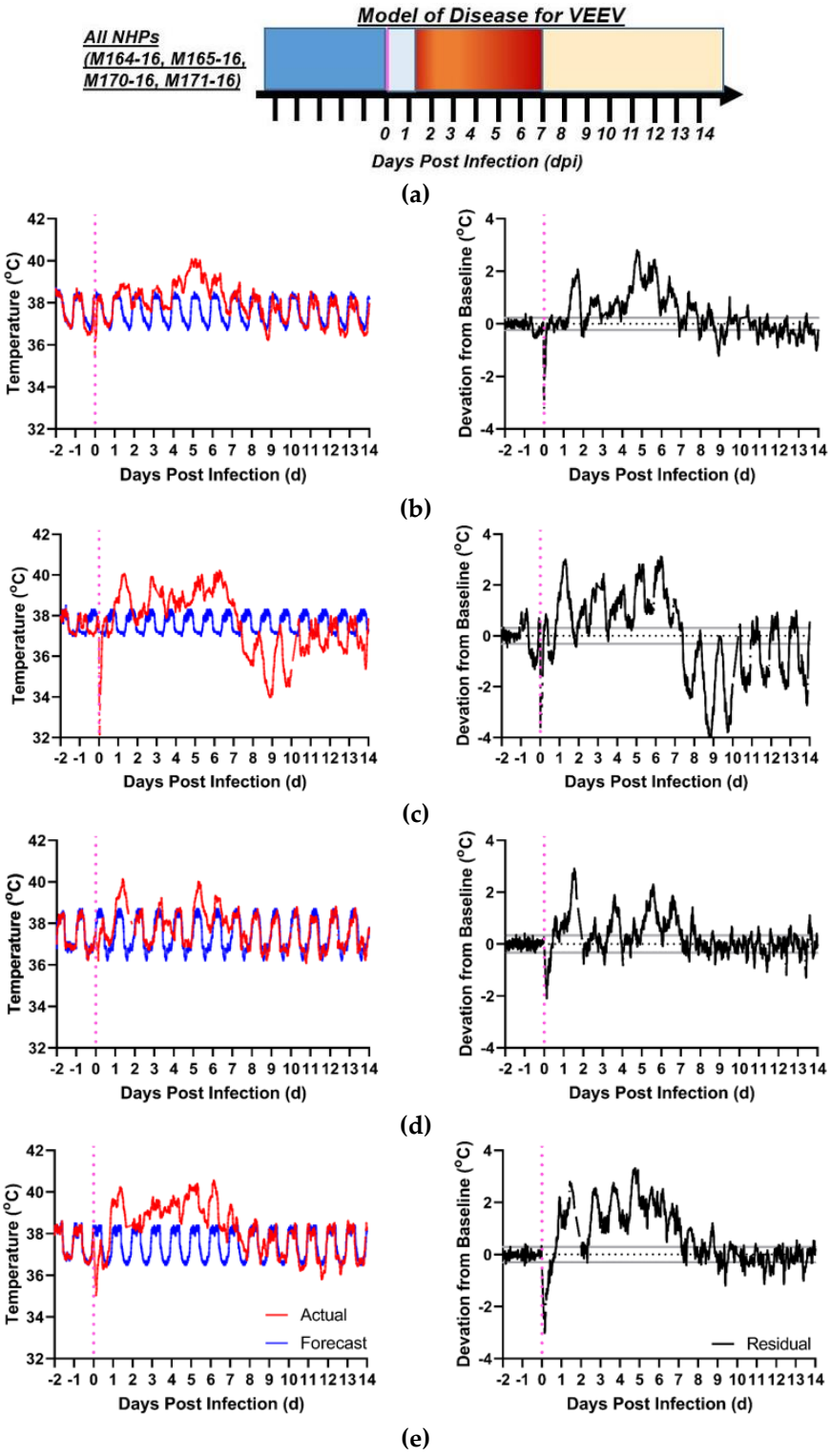

Figure 6. VEEV disease in macaques. Shown is the model of disease for **(a)** VEEV-exposed macaques over days post-infection (x-axis); all macaques developed febrile encephalitic disease. Deep blue denotes pre-infection baseline period, vertical magenta line denotes time of infection, powder blue defines post-infection period before the onset of fever, red signifies the febrile post-infection period, and yellow signifies recovery period after febrile illness subsides. Actual and forecasted temperature profiles for female macaques: **(b)** M164-16, **(c)** M165-16, and male macaques: **(d)** M170-16 and **(e)** M171-16. Red: Actual Temperature (°C), Blue Forecasted Temperature (°C) from ARIMA modeling, Black: Residual Values (°C) (deviations from forecasted baseline). Gray Lines: upper/lower bounds for residuals Magenta: aerosol challenge.

Preprints (www.preprints.org) | NOT PEER-REVIEWED | Posted: 11 October 2019 doi:10.20944/preprints201910.0121.v1

Peer-reviewed version available at Pathogens 2019, 8, 240; doi:10.3390/pathogens8040240

QT-intervals of the VEEV-infected macaques decreased during the post-infection period, and remained decreased during the febrile period; examination of QT-interval traces (Figure 7a) reveals that in two macaques (M165-16, M171-16) the QT-interval remained decreased during the recovery period, but for the other two in the cohort (M164-16, M170-16), the QT-interval returned to baseline during recovery. The daily QT-interval aggregate (Figure 7b) demonstrates that the QT-interval exhibited a sustained decrease beginning from the immediate post-infection period through the febrile period, until the beginning of the designated recovery period at 8 dpi; repeated measures ANOVA indicated statistically significant departures from baseline QT-interval in all four macaques (Table 3, $p<0.05$).

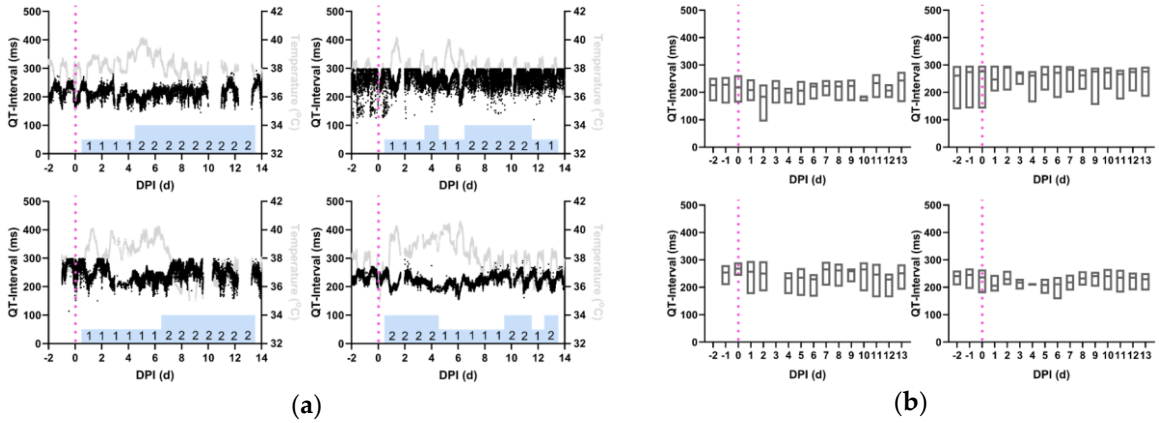

(a) (b)

Figure 7. Reduction in QT-Interval during the febrile period in macaques infected with VEEV. Shown are the profiles **(a)** of QT-Interval derived from 1-minute average measurements for four individual macaques infected with VEEV. Black: QT-Interval (ms), Gray: Temperature (°C), and Magenta: aerosol challenge. Blue Bars: Neurological score on corresponding day. **(b)** Average daily QT-Interval measurements, from repeated measures ANOVA, depicted in with boxes delimited by interquartile range and center line signifying median value. For **(a)** and **(b)**, Top Left: M164-16, Bottom Left: M165-16, Top Right: M170-16, Bottom Right: M171-16.

The RR-intervals of macaques infected with VEEV (Figure 8a) demonstrated decreases in all macaques beginning in the immediate post-infection, and remained persistently low throughout the recovery period. This effect is visible in the median RR-interval in aggregate data (Figure 8b), in

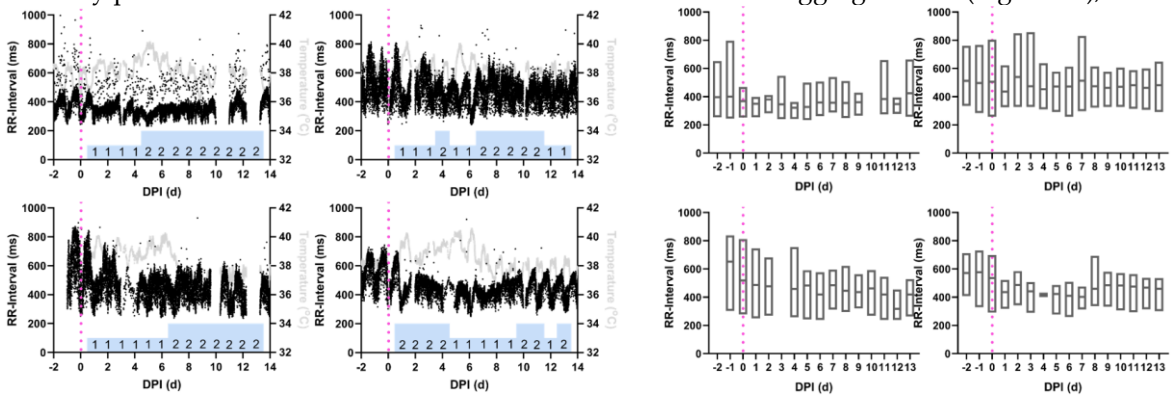

(a) (b)

Figure 8. RR-Interval decreases and remains decreased in macaques with VEEV encephalitis. Shown are the profiles **(a)** of RR-Interval derived from 1-minute average measurements for four individual macaques infected with VEEV. Black: RR-Interval (ms), Gray: Temperature (°C), and Magenta: aerosol challenge. Blue Bars: Neurological score on corresponding day. **(b)** Average daily RR-Interval measurements, from repeated measures ANOVA, depicted in with boxes delimited by interquartile range and center line signifying median value. For **(a)** and **(b)**, Top Left: M164-16, Bottom Left: M165-16, Top Right: M170-16, Bottom Right: M171-16.

Preprints (www.preprints.org) | NOT PEER-REVIEWED | Posted: 11 October 2019 doi:10.20944/preprints201910.0121.v1

Peer-reviewed version available at Pathogens 2019, 8, 240; doi:10.3390/pathogens8040240

which the RR-interval can be seen to trend downward beginning in the immediate post-infection period at 0 or 1 dpi (Table 4, $p<0.05$).

The HRV for the VEEV-infected macaques show in aggregate that when scatter plots of daily HRV distributions are superimposed and color-coded by pre-infection, post-infection, febrile, and recovery periods (Figure 9), the distribution of ordered pairs contracts, and remains contracted well after the febrile period. When decomposed into Poincaré plots by day post infection, representative of each disease period (Supplemental Figure A3), the persistence of the decrease in heart rate variability is even more apparent. As with the related RR-interval, all macaques experienced this effect.

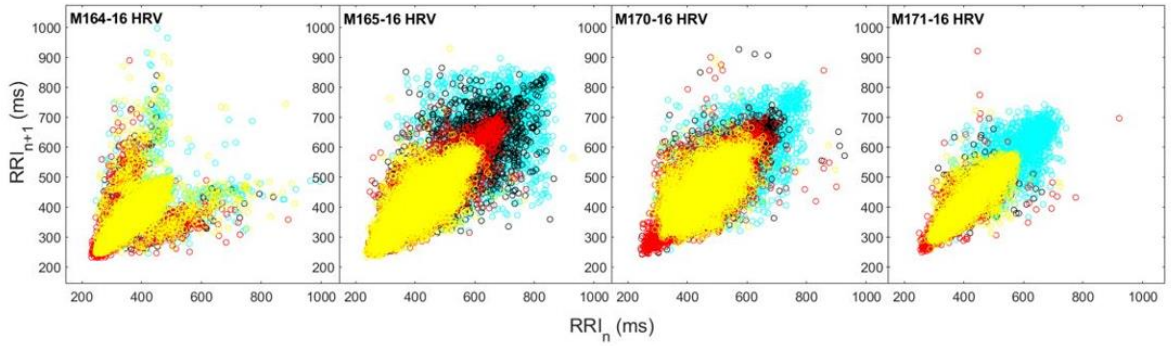

Figure 9. Heart Rate Variability Decreases during the febrile period in macaques infected with EEEV. Distributions of heart rate variability of each EEEV-infected macaque are plotted in aggregate EEEV and color-coded by disease period (Cyan: Pre-Infection, Black: Post-Infection, Red: Febrile, Yellow: Recovery).

2.3. Frequency Spectrum Analysis

Using Fast Fourier transformation (FFT), pre-/post-infection and febrile periods were distinguishable from one another in the macaque subjects with severe courses of disease. The fundamental frequency, defined as the first local maximum in the frequency spectrum, of each metric was computed in cycles per day (cpd). Patterns of change in the frequency spectra varied little between ECG metrics, especially between those that co-varied; for instance, metrics associated with heart rate, such as RR-interval, exhibited similar trends with respect to how the fundamental frequencies changed between pre-, post-, and febrile periods. The amplitude of the frequency spectrum plots was not significant, as magnitude squared (ms^2 in this case) determined by the number of points fed into the FFT and the amplitude of the original signal in the time domain. Fundamental frequencies for the RR-interval, as a representation of the overall trend of frequency changes, are tabulated in Table 5.

Prior to infection, the fundamental frequency for RR-interval was different between macaques; however, most fell into a fairly narrow range. Macaques infected with EEEV that did not develop severe disease saw no significant changes in RR-I fundamental frequencies post-infection (Table 5). Changes in RR-I fundamental frequencies were much larger in severely diseased macaques. In the EEEV-infected macaques with severe disease, the post-infection frequency increased to 0.879 and 0.769 cpd, then decreased to 0.571 and 0.549 cpd in the febrile period although this was still elevated compared to baseline. Values for VEEV were larger due to the extended time periods used for analysis. Examination of fundamental frequencies identified relatively high cyclic rates in the VEEV cohort with differences based on sex: 5.97 cpd and 11.25 cpd for female and male monkeys, respectively, at pre-infection. For both females and males, the fundamental frequencies increased after VEEV infection and then dropped below baseline levels in the febrile period with the sharpest decline in the male macaques. With the onset of the designated recovery period in VEEV, the fundamental frequency of the latter period, when body temperatures largely returned to normal, the fundamental frequencies in

Preprints (www.preprints.org) | NOT PEER-REVIEWED | Posted: 11 October 2019 doi:10.20944/preprints201910.0121.v1

Peer-reviewed version available at Pathogens 2019, 8, 240; doi:10.3390/pathogens8040240

the VEEV-infected macaques remained lower than pre-infection although the greatest reduction was seen in the males.

Table 5. Fundamental Frequencies of EEEV and VEEV Courses of Infection. This table documents fundamental frequencies observed in the ECG metric of RR-Interval. Disease periods are separated into pre-infection, post-infection (outside of any febrile period), and febrile periods for EEEV VEEV. Recovery periods were also included when applicable, specifically in the case of the VEEV cohort. Fundamental frequencies are displayed in cycles per day (cpd). Values for VEEV are larger due to the extended time periods used for analysis; the values in parentheses are normalized to the first harmonic value for the purposes of comparison to EEEV frequency values. Italicized values represent animals with fatal courses of disease.

Virus	Macaque	Sex	Pre-Infection Frequency	Post-Infection Frequency	Febrile Period Frequency	Recovery Period Frequency
EEEV	*161-16*	*M*	*0.395*	*0.879*	*0.571*	
	163-16	*M*	*0.242*	*0.769*	*0.549*	
	160-16	M	0.351	0.242		
	162-16	M	0.307	0.351		
VEEV	164-16	F	5.974 (0.373)	11.070 (0.275)	4.393 (0.275)	3.514 (0.220)
	165-16	F	5.974 (0.373)	11.070 (0.286)	4.568 (0.286)	3.514 (0.220)
	170-16	M	11.245 (0.351)	13.881 (0.434)	4.217 (0.132)	3.163 (0.099)
	171-16	M	11.245 (0.351)	13.705 (0.428)	5.271 (0.165)	3.163 (0.099)

3. Discussion

3.1. QRS Complexes

As the QRS interval corresponds to ventricular depolarization in the heart and therefore the speed with which ventricular contraction occurs, a widened QRS complex could point to electrolyte imbalances such as hypokalemia. Clinical observations noted that both severely diseased EEEV-infected macaques had decreased water intake during the febrile period and signs of dehydration. However, blood chemistry analysis obtained at baseline, during aerosol, and at necropsy did not bear out this hypothesis, as potassium levels were within normal limits (3.5-5 mEq), leaving the question open as to whether autonomic dysregulation is responsible for the pathological phenomenon observed. The lack of blood chemistry between infection and necropsy means that the possibility of electrolyte balance dysregulation cannot be completely ruled out. Recent investigation has suggested that autonomic modulation of heart rate regulation can lead to morphological changes in the QRS complex, with shorter QRS complexes representing a shift towards sympathetic predominance [37]. However, in the macaques in which this occurred, the finding was more likely a covariate of an increased heart rate due to febrile illness.

3.2. QT-Intervals

The QT-interval represents the interval of time between the Q-Wave (beginning of ventricular depolarization) and the T-Wave (ventricular repolarization) of the ECG. The finding of decreased QT-intervals in the EEEV-exposed macaques with severe disease, again, represents an anomaly in that though the QT-interval is decreased, the QRS complex, which comprises a segment of the QT-interval, is increased. The QT-interval is of particular interest for the testing of therapeutic compounds, due to the extent to which certain small molecule drug candidates can affect the QT-interval. Ion channels in the myocardium can be affected by off-target effects, and this represents concern for potential pharmacological intervention [38]. However, pre-clinical studies in uninfected

Preprints (www.preprints.org) | NOT PEER-REVIEWED | Posted: 11 October 2019 doi:10.20944/preprints201910.0121.v1

Peer-reviewed version available at Pathogens 2019, 8, 240; doi:10.3390/pathogens8040240

animal models should mitigate the potential for such an eventuality. Perhaps the most thought-provoking aspect of the QT-interval effects resides in the alterations to diurnal variation during and sometimes after the period of febrile illness, a finding mirrored in the upcoming discussion of the RR-interval and heart rate variability.

3.3. RR-Interval, Heart Rate Variability, and Frequency Spectrum Analysis

The RR-interval denotes the interval of time between two heartbeats, while heart rate variability (HRV) represents the variation in the time interval between heartbeats, expressed in milliseconds [39]. The notion that RR-interval and HRV can illustrate the circadian rhythm of autonomic regulation has been well characterized [40-42]. Changes in HRV have comprised the subject of study by multiple authors who have associated alterations in the RR-interval and HRV with pathology such as diabetes mellitus and its associated diabetic neuropathy, heart failure, myocardial infarction, and other chronic conditions [40,43,44]. Additionally, more recent studies have suggested a link not only between inflammatory markers and HRV [45], but also between changes in the RR-interval and heart rate variability in a number of diseases of infectious origin [46-48].

For both VEEV-infected and severely EEEV-infected macaques, there was a decrease in the RR-Interval in the febrile period. For severe EEEV-infection, the decrease was greater, with a more complete loss in diurnal variation. Subsequent work with macaques challenged with EEEV (not published) demonstrates that the EEEV macaques with no overt clinical signs of disease are indeed infected, as determined by plaque assay and antibody neutralization titers from plasma obtained from serial blood draws following the aerosol challenge. Therefore, as the EEEV-challenged macaques with nonsevere disease also have limited to no changes in RR-interval as depicted in daily Poincaré plots, this effect can therefore distinguish severe from nonsevere courses of disease. RR-interval remained persistently low in all four VEEV-infected macaques even through the recovery period. Despite recovery from encephalitic disease, the results suggest that infection with VEEV may have altered the homeostatic set point of autonomic regulation, as previously reported in the literature [12,18,49].

The fundamental frequency represents the frequency with which the original time domain signal (the ECG metric) repeats, typically multiple times per day due to idiosyncrasies in the autonomic regulation of cardiac function. Although the fundamental frequency is what was used as the benchmark, subsequent local maxima are registered as *nth* harmonics, or subsequent echoes, of the fundamental frequency. Frequency spectrum analysis reveals similar trends over different periods of EEV disease courses; post-infection, the fundamental frequencies of the ECG metrics typically increase, then decrease during the febrile period in individuals with severe disease.

In the context of frequency spectrum analysis, for macaques with severe courses of EEEV, the fundamental frequencies of the RR-interval increased between pre-infection, the latency period, and febrile disease, whereas the fundamental frequencies of macaques with nonsevere courses of EEEV remain relatively unchanged. This result corroborates the value of RR-interval in distinguishing between severe and nonsevere cases of EEEV and highlights the capacity of frequency spectrum analysis to perform this distinguishing function. For VEEV, the fundamental frequencies of the RR-interval increased post-infection during the short latency period, then decreased during the onset of febrile illness. During the recovery period, the fundamental frequency proceeded to decrease again as the permanence of the decreased RR-interval, plotted in Poincaré plots in Supplemental Figure A4, and diminished heart rate variability for the VEEV-exposed cohort is recapitulated in Table 5 by the frequency spectrum analysis, suggesting a real physiological rather than artifactual basis for these results. The existence of post-infection changes in the fundamental frequencies in subjects who survived EEEV challenge suggests that neurological sequelae could occur even without a strong febrile response or obvious clinical signs, sequelae that could have long term health consequences.

Preprints (www.preprints.org) | NOT PEER-REVIEWED | Posted: 11 October 2019 doi:10.20944/preprints201910.0121.v1

Peer-reviewed version available at Pathogens 2019, 8, 240; doi:10.3390/pathogens8040240

3.4. Limitations and Future Work

We do acknowledge that there is a shortfall in investigating the electrocardiographic implications of the dose-response relationship due to the small sample sizes, a limitation partially offset by the sheer volume of data obtained from each subject. The potential confounding effect of subject sex likewise presents a limitation; the EEEV cohort was entirely male, while the VEEV cohort was split between the sexes. Baseline metrics varied significantly between individual macaques, although all baseline measures fell within normal limits. At this juncture, it is not clear whether the results reported here are applicable to other viral encephalitides. Direct application of these analyses in a human clinical context may suffer from limited generalizability, based on the variability in baseline ECG metrics between individual macaques and baseline ECG data would not be available for most human patients.

There are a number of remaining questions, including the following: do sex-based differences in electrocardiographic signatures precipitate effects on the response to infection by aerosol route, and if so, how does the periodicity of hormonal changes, for example, modify the outcome, especially with respect to the loss of circadian variation seen in all signals? Perhaps body weight or animal size may exert an effect on the electrocardiographic metrics not only in baseline data, but also in the post-infection period response, through the febrile period. A decrease in RR-Interval during the febrile period appears to be a generalizable phenomenon to other severe, acute infectious diseases (D.S. Reed, manuscript in preparation) although it is not clear if these other severe infections penetrate the CNS particularly when the route of exposure is also aerosol. The other parameters noted here (QT-Interval, QRS) may be specific to viral encephalitis. Finally, it may be helpful to determine whether a dose-dependent relationship exists between the manifestation of electrocardiographic changes and the dose of virus received, or between the immune response observed, or whether the ECG effects observed are binary once exposure exceeds a threshold dose. The results described appear to support the latter theory; while these results may not be specific to viral encephalitides and may not supplant fever as a biomarker for the initiation of treatment, they may serve as useful predictors of outcome. Further investigation with electroencephalography can better determine whether the differences observed between sexes are responsible for the dichotomies observed in the results, and can help to establish whether the observed ECG effects stem from a basis in autonomic dysregulation, from direct viral infection, the immune response to infection, or a combination of these factors.

Future work may improve the utility of ECG data to provide specific profiles and prognosticators of disease. Dimension reduction can be carried out among covarying metrics for the purposes of principal component analysis to provide a more robust form of prognostication. In conjunction with analysis of electroencephalography and other telemetric modalities, such methods could prove a powerful tool, followed in real time or quasi-real-time by lab staff, for investigating both viral pathogenesis and developing therapeutics and countermeasures against EEV aerosol infection. Whether EEVs directly affect cardiac responses as captured by electrocardiography metrics with respect to damage to the myocardial syncytium versus the disruption of autonomic outflow requires further study and remains an area of continuing investigation.

4. Materials and Methods

4.1 Statement on Rationale, Use, and Care of Animals

This study was approved by the University of Pittsburgh IACUC (Protocol #16026773) and was fully compliant with rules, regulations, and recommendations stipulated by the Animal Welfare Act Regulations and the Guide for the Care and Use of Laboratory Animals, [50]. The University of Pittsburgh, which includes a regional biocontainment laboratory (RBL), is accredited by the Association for Assessment and Accreditation of Laboratory Animal Care (AAALAC). The rationale for the development of a nonhuman primate (NHP) model of inhalational EEV disease fulfills the necessity criteria outlined by the FDA Animal Rule [29,51,52]. The cynomolgus macaque (*Macaca fascicularis*) has served as a model organism for EEVs since the discovery of these viruses in the 1930s

Preprints (www.preprints.org) | NOT PEER-REVIEWED | Posted: 11 October 2019 doi:10.20944/preprints201910.0121.v1

Peer-reviewed version available at Pathogens 2019, 8, 240; doi:10.3390/pathogens8040240

[6,53]. Additionally, this species provides distinct advantages over rodents due to the greater anatomical and physiological similarity of macaques to humans [35,36,54,55]. Infection of macaques by subcutaneous and aerosol routes of infection can reproduce CNS lesions that resemble those produced during EEV infection in human cases [35,36,56,57]. The augmentation of this well-established animal model for encephalitic disease by the respiratory route remains paramount for the recapitulation of clinical markers and histopathology of encephalitic disease in the context of the development of improved vaccines against aerosol-induced disease.

Cynomolgus macaques were singly housed for the duration of these studies. Subjects were monitored on a daily basis and clinically scored according to a series of ordinal scales for the following categories: neurological, activity, and temperature [35,36,58]. The neurological scoring scale ranged from 1-6 and accounted for signs such as tremor, gait imbalance, nystagmus, head pressing, seizures, and coma. The activity score ranged from 1-6 and accounted for mental status as determined by posture, facial expressions, responses to stimuli, and interactions with observers. Finally, the temperature scale ranged from 1-6, accounted for core temperature, and gauged for fever and hypothermia. The ordinal scoring scales were summed and the cumulative score was used to determine whether a macaque warranted more frequent observation or was at risk of imminent death which would require immediate euthanasia. Excreta and food/fluid intake were also monitored daily.

4.2 Animal Model Telemetry Implantation

The macaques used in this study were implanted intra-abdominally with Data Sciences International (DSI, St. Paul, MN) radiofrequency transmitters (DSI Model No. M01) by a DSI veterinarian at Covance Laboratories (Princeton, NJ). In preparation for surgery, the macaques were each administered 25mg/kg cefazolin (1st-generation cephalosporin) for infection control and 1mg/kg ketoprofen for analgesia, and the incision site, 5 cm superior to the anterior superior iliac spine, was shaved. Macaques were anesthetized with 10mg/kg ketamine with continuous IV administration of 3% normal saline via the great saphenous vein. Isoflurane (2%v/v) was then administered for continuous anesthesia with 4.0-4.5L/min of O_2. The incision site was draped and sterilized with chlorhexidine antiseptic and 70%v/v isopropyl alcohol. A 5 cm incision was made parallel to the midline, into which the implant was inserted. ECG leads were sutured in place, one under the right pectoralis muscle and one parallel to the left inguinal area, approximating Lead II placement in a 12-lead ECG [59]. The incision was closed with a simple interrupted stitch. Post-operatively, each macaque was eligible for 3 days' administration (PRN) of buprenorphine for analgesia and received 5 days' administration (BID) of cefazolin for infection control.

4.3 Virus Culture and Dose Determination

Virus cultures were conducted as described in the literature [60]. The EEEV and VEEV isolates used in this study were single passages of infectious clones generated from human isolates: V105 (EEEV) and INH-9813 (VEEV-IC). For both alphaviruses, stocks were generated through construction of cDNA libraries; capped, infectious viral RNAs were generated by *in vitro* RNA synthesis from linearized cDNA plasmid template genomes that were electroporated into baby hamster kidney (BHK-21, ATCC) cells (Klimstra, manuscript in preparation). The supernatant was clarified by centrifugation between 18-24 hours post-electroporation, and single-use aliquots were stored at -80°C as zero-passage (p0) stocks. The p0 stocks were titered by standard plaque assays on BHK-21 cells and used to infect Vero cells (ATCC CCL-81) at a multiplicity of infection of 10 in roller bottles. At 18-24 hours post-infection, the supernatant was clarified by centrifugation and subjected to sucrose purification. The supernatant was layered over a 20/60% sucrose cushion and ultracentrifuged. The interface between the 20/60% sucrose cushion was collected and diluted in 10mM Tris, 1mM EDTA, 100mM NaCl–STE 10X NaCl (TNE) buffer. The interface was then layered over 20% sucrose and again ultracentrifuged to pellet the virus. The pelleted virus was resuspended in Opti-MEM® Reduced Serum Medium (ThermoFisher, Catalog No. 31985-070) and single-use aliquots were stored at -80°C. The virus stock (passage 1), nebulizer samples, and aerosol samples

Preprints (www.preprints.org) | NOT PEER-REVIEWED | Posted: 11 October 2019 doi:10.20944/preprints201910.0121.v1

Peer-reviewed version available at Pathogens 2019, 8, 240; doi:10.3390/pathogens8040240

were titered using standard plaque assays on BHK-21 cells and the aerosol LD_{50} confirmed in mice before use in macaque studies.

4.4 Aerosol Exposure of Macaques to EEVs

For each exposure, aerosol generation was performed in a modified Class III biosafety cabinet [61]. Aerosol exposures were performed under the control of the Aero3G aerosol management platform (Biaera Technologies, Hagerstown, MD) as previously described [62]. Macaques were anesthetized with 6 mg/kg Telazol® (Tiletamine HCl / Zolazepam HCl). Each macaque was then weighed, bled, and transported to the modified Class III biosafety cabinet using a mobile transport cart. The macaque's head was placed inside an acrylic head-only exposure chamber. Jacketed External Telemetry Respiratory Inductive Plethysmography (JET-RIP; DSI) belts were placed around the abdomen and chest of the macaque and calibrated to a pneumotach. This allowed monitoring and recording of respiratory function via the Ponemah software platform (DSI) during the aerosol [63]. EEV aerosols were generated using an Aeroneb vibrating mesh nebulizer (Aerogen, Chicago, IL) as previously described [64]. Exposures were 10 minutes in duration. To determine inhaled dose, aerosol sampling was performed during each exposure with an all-glass impinger (AGI; Ace Glass, Vineland, NJ). Particle size was measured once during each exposure at 5 minutes using an Aerodynamic Particle Sizer (TSI, Shoreview, MN). A 5-minute air wash followed each aerosol before the macaque was removed from the cabinet, and transported back to its cage and observed until fully recovered from anesthesia.

4.5 Electrocardiography Data Collection

Electrocardiography, activity, and temperature data were collected continuously from implanted macaques for at least two days before aerosol exposure and for the duration of the disease course post-exposure. An example of a raw ECG trace is shown in Supplemental Figure A4. A computer connected to a communication link controller (CLC; DSI) collected signals from the implanted macaques by way of transceivers mounted in the room. Video cameras were positioned to record macaque behavior and were programmed to record continuously, synchronously, alongside the telemetry data. Because of the amount of telemetry and video data generated daily, the system had to be manually stopped and restarted every morning. The Ponemah software package (v.5.2; DSI) provides a graphic user interface that presents a unified, multichannel display of the data collected from the M01 implants' sensors. For analysis, data were read either in raw form (.RAW file extension) or reviewed in common spreadsheet, statistical analysis, and plotting programs. Body temperature and electrocardiographic measures including heart rate were sampled at 10 Hz and recorded every 5 seconds [65]. For fever, a Box-Jenkins ARIMA model was used to predict 15-minute average body temperature from baseline data; significant deviations (3 times the square root of the residual sum of squares) of actual from predicted temperatures were scored as fever. Fever duration was calculated as the number of fever points divided by 4 (the number of points per hour); fever severity was measured as 'fever-hours', the summation of residual elevated temperatures divided by 4. ARIMA analysis was done using Number Cruncher Statistical Systems (NCSS) 2007 software. Electrocardiography metrics studied are displayed in Supplemental Table A1. Standard deviations of these metrics were measured and recorded at the same sampling frequencies as well.

4.6 Electrocardiography Analysis Methods

Disease courses were defined by the appearance of fever during the clinical observation period; for each cohort of EEV-infected macaques, periods were established based on the timing of infection and fever: pre-infection, post-infection (prior to fever onset), febrile period, and recovery, when applicable. These periods were constructed according to the markers for fever explained above. Analyses of electrocardiography metrics were carried out by considering the median daily electrocardiographic metric of interest or by considering the aggregate median electrocardiographic metric of interest over the periods previously defined.

Electrocardiographic metrics were sampled from the raw data at a rate of one sample per minute for 1440 data points per day to reduce the computational burden on the analytical software

Preprints (www.preprints.org) | NOT PEER-REVIEWED | Posted: 11 October 2019 doi:10.20944/preprints201910.0121.v1

Peer-reviewed version available at Pathogens 2019, 8, 240; doi:10.3390/pathogens8040240

and to reduce the impact of noise on producing artificially significant results. Statistical analyses were performed in two stages: preliminary analysis of temperature and activity were performed alongside the collection of data, with limited analysis of the raw ECG traces. A more comprehensive statistical analysis was performed with a within-subjects repeated measures ANOVA approach. Due to significant variability in baseline metrics, the baseline period for each macaque served as its own control for this study. All significance levels utilized were $\alpha<0.05$. Heart rate variability was mapped as described by Golinska, and Poincaré plots were constructed according to guidelines described by Henriques, et al [66,67].

To examine circadian changes in the electrocardiographic data, frequency spectrum analysis was performed by use of the fast Fourier transform (FFT). Time-series of the electrocardiographic metrics were decomposed into linear combinations of basic trigonometric functions. The frequencies of these trigonometric functions produces a discrete spectrum, with each frequency point representing a component frequency of the original time-series. The fundamental frequency, or the first defining frequency peak (local maximum) in the frequency spectrum window, in units of cycles per day, explored the differences in pre-/post-infection, febrile, and recovery periods. Subtle changes in the number of cycles per day, or the subcomponents of the normal cyclic rates of electrocardiographic metrics, were quantified and visualized. These procedures were carried out in MATLAB 2018b (Mathworks, Natick, MA) with the use of native frequency analysis algorithms.

5. Conclusions

This work was performed to further develop and characterize the macaque model for aerosol exposure to EEVs. In agreement with what we saw previously, fever was a prominent indicator of EEV disease. Across both EEEV and VEEV, it is notable that the macaques who succumbed to severe disease had a maximum temperature difference from predicted of 4.0°C or higher while all of those that survived infection had maximum temperature differences less than 4.0°C from predicted. The goal of these studies was to determine whether other physiological parameters might be suitable as biomarkers or indicators for future efficacy studies. The augmented animal model might suffice to evaluate therapeutic compounds under the FDA Animal Rule. Although these are encephalitic viruses, heart function is controlled by the nervous system so we surmised that ECG metrics would be useful for this objective. Indeed, the data suggests that ECG metrics are useful for this purpose, but the ECG metric chosen will be dependent on the particular alphavirus used and will likely need to be paired with body temperature to paint a complete picture of the disease and outcome in macaques. The most prominent set of significant electrocardiographic metrics that distinguish and characterize both EEEV and VEEV disease courses consist of QRS complexes, QT-interval, and RR-interval.

Preprints (www.preprints.org) | NOT PEER-REVIEWED | Posted: 11 October 2019 doi:10.20944/preprints201910.0121.v1

Peer-reviewed version available at Pathogens 2019, 8, 240; doi:10.3390/pathogens8040240

582

583 **Supplementary Materials:** The following are available online, Figure S1: Representative Poincaré Plots for
584 Nonsevere EEEV Infection Cohort, Figure S2: Representative Poincaré Plots for Severe EEEV Infection Cohort,
585 Figure S3: Representative Poincaré Plots for VEEV Infection Cohort, Figure S4: Example ECG Trace, Table S1:
586 Electrocardiographic Metrics.

587 **Author Contributions:** Conceptualization, H.M., D.R, A.H, and W.K.; methodology, H.M.; software, H.M.;
588 validation, H.M., and D.R.; formal analysis, H.M. and D.R.; investigation, H.M. and D.R.; resources, A.H., D.R.,
589 and W.K.; data curation, H.M., J.L., and K.O.; writing—original draft preparation, H.M.; writing—review and
590 editing, H.M., D.R., A.H., and W.K.; visualization, H.M. and D.R.; supervision, D.R. and A.H.; project
591 administration, A.H.; funding acquisition, A.H., D.R., and W.K.

592 **Funding:** This research was funded by Defense Threat Reduction Agency (DTRA), grant number
593 W911QY-15-1-0019 and The APC was funded by the same. Disclaimer: This project was sponsored by the
594 Department of the Army, U.S. Army Contracting Command, Aberdeen Proving Ground, Natick Contracting
595 Division, Ft. Detrick, MD under grant #W911QY-15-1-0019. Research was conducted in compliance with the
596 Animal Welfare Act and other Federal statutes and regulations relating to animals and experiments involving
597 animals and adheres to principles stated in the Guide for the Care and Use of Laboratory Animals, National
598 Research Council, 1996. The facility where this research was conducted is fully accredited by the Association for
599 Assessment and Accreditation of Laboratory Animal Care International. Opinions, interpretations, conclusions,
600 and recommendations are those of the author and are not necessarily endorsed by the Department of Defense.

601 **Acknowledgments:** This work was funded by the Defense Threat Reduction Agency Grant #W911QY-15-1-0019
602 and is sponsored by the Department of the Army, U.S. Army Contracting Command, Aberdeen Proving
603 Ground, Natick Contracting Division, Ft. Detrick Maryland. Any opinions, findings, and conclusions or
604 recommendations expressed in this material are those of the author(s) and do not necessarily reflect the position
605 or the policy of the Government and no official endorsement should be inferred. Special thanks to members of
606 the Hartman and Klimstra labs at the University of Pittsburgh, especially Cynthia M. McMillen, Stacey Barrick,
607 Theron Gilliland, Jr., Aaron Walters, and members of the Division of Laboratory Animal Resources, especially
608 Reagan Walker. This manuscript represents a subsection of work performed by Henry Ma for the completion of
609 a master's thesis [68].

610 **Conflicts of Interest:** The authors declare no conflict of interest. The funders had no role in the design of the
611 study; in the collection, analyses, or interpretation of data; in the writing of the manuscript, or in the decision to
612 publish the results. None of the submitted work was carried out in the presence of any personal, professional,
613 or financial relationships that could be potentially construed as a conflict of interest; none of the authors listed
614 owns controlling interest in any of the vendors or suppliers listed in this manuscript.

615

616

617

618

619

620

621

622

623

624

625

626

627

628

629

Preprints (www.preprints.org) | NOT PEER-REVIEWED | Posted: 11 October 2019 doi:10.20944/preprints201910.0121.v1

Peer-reviewed version available at Pathogens 2019, 8, 240; doi:10.3390/pathogens8040240

630

631 **Appendix A – Supplementary Figures and Tables**

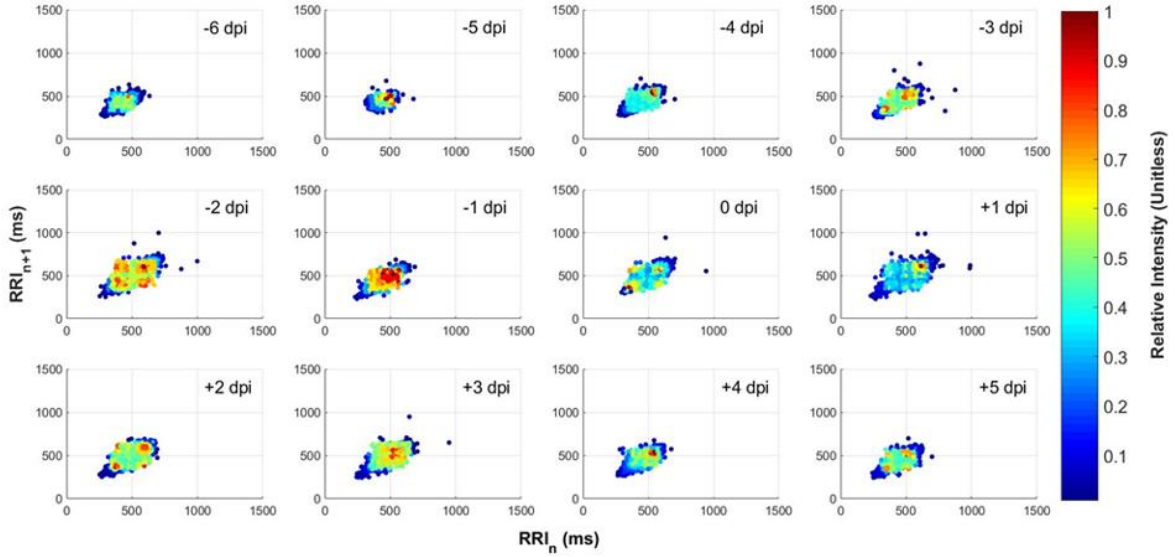

632 **Supplemental Figure A1. Representative Poincaré Plots for Nonsevere EEEV Infection Cohort.**
633 Representative daily Poincaré plots for a macaque with nonsevere EEEV infection (M160-16).

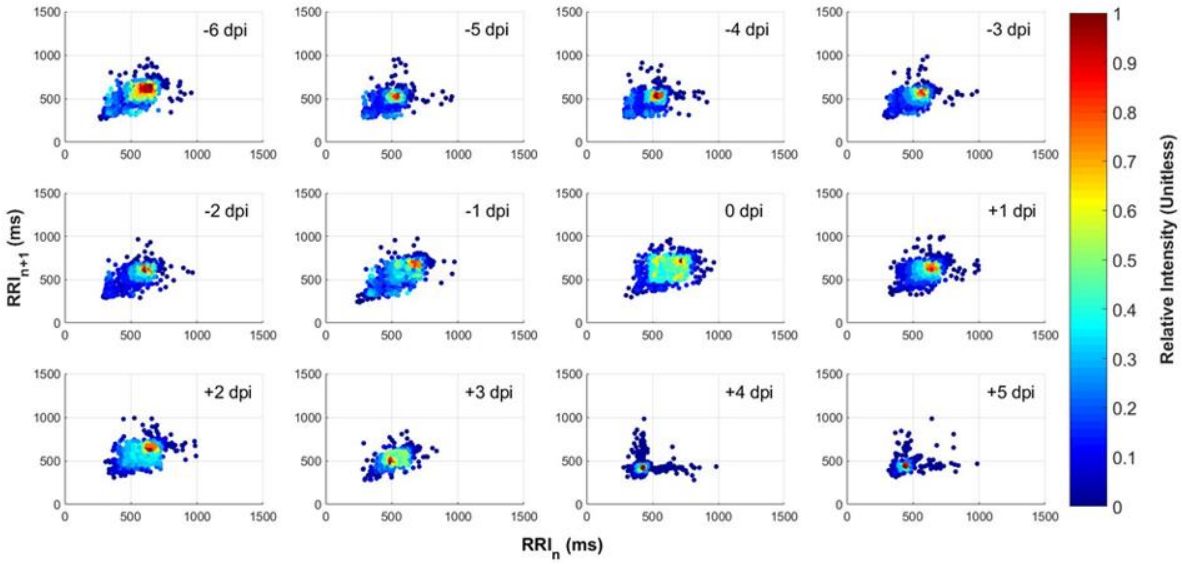

634 **Supplemental Figure A2. Representative Poincaré Plots for Severe EEEV Infection Cohort.**
635 Distributions of heart rate variability of each EEEV-infected macaque are plotted in aggregate EEEV
636 and color-coded by disease period (Cyan: Pre-Infection, Black: Post-Infection, Red: Febrile, Yellow:
637 Recovery).

Preprints (www.preprints.org) | NOT PEER-REVIEWED | Posted: 11 October 2019 doi:10.20944/preprints201910.0121.v1

Peer-reviewed version available at Pathogens 2019, 8, 240; doi:10.3390/pathogens8040240

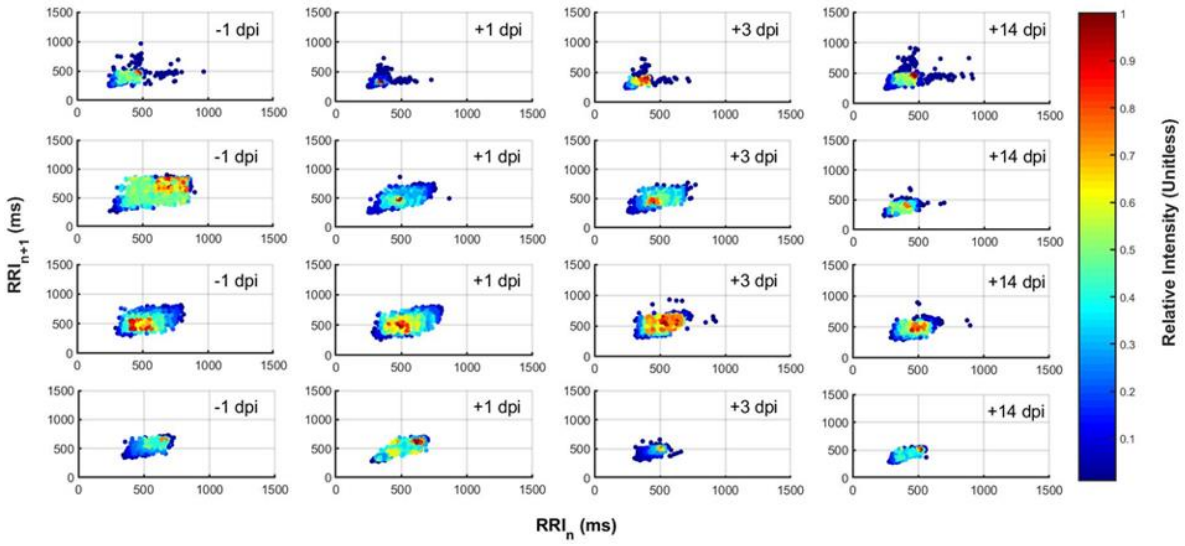

Supplemental Figure A3. Representative Poincaré Plots for VEEV Infection Cohort. Representative daily (from -1, +1, +3, and +14 dpi) Poincaré plots for each macaque in the VEEV infection cohort (top to bottom: M164-16, M165-16, M170-16, and M171-16) show diminished range of HRV following infection that persists into the recovery period.

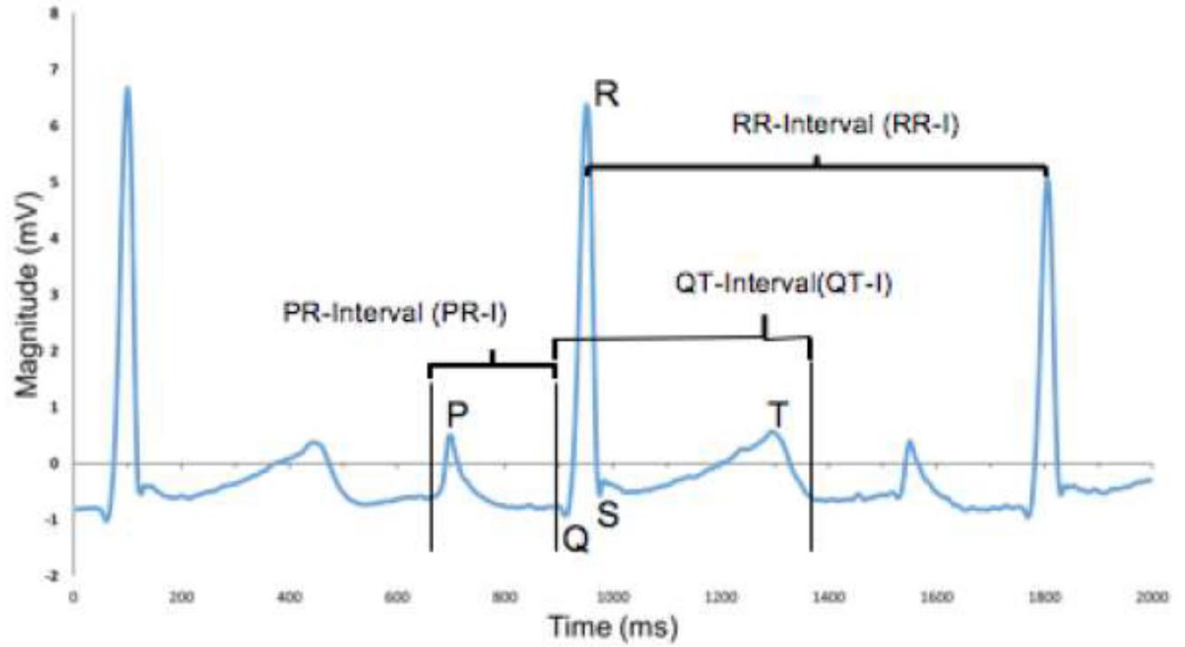

Supplemental Figure A4. Example ECG Trace. Shown is a sample ECG trace from a macaque in this study. The electrocardiogram generated by a single heartbeat provides the PQRST profile (marked) of an atrial and ventricular contraction and repolarization. Different segments of the waveform serve as key metrics that may inform upon underlying cardiac anatomical and physiological status. The P wave corresponds to the depolarization of the atria, the QRS complex corresponds to both ventricular depolarization and atrial repolarization, and the T wave represents ventricular repolarization. QRS complex is defined by the time period transited by the peak between points Q and S.

Preprints (www.preprints.org) | NOT PEER-REVIEWED | Posted: 11 October 2019 doi:10.20944/preprints201910.0121.v1

Peer-reviewed version available at Pathogens 2019, 8, 240; doi:10.3390/pathogens8040240

652 **Table A1. Electrocardiographic Metrics.** Abridged list of metrics under study.

Electrocardiography Metric	*Abbreviation*	*Significance*	*Units*
Arrhythmic Beat Detection	BAD	The number of arrhythmic beats detected during a logging period.	*Count*
Heart Rate	HR	Number of heartbeats per minute.	*bpm*
Heart Rate Variability	HRV	RR-Interval matched with RR-Interval$_{n+1}$, plotted as an ordered pair.	*ms, Unitless*
Maximum Voltage Derivative of R-Wave	MxdV	Maximum rate of change of ECG trace at R-Wave.	*mV/ms*
Noise in ECG Trace	Noise	Approximation of noise level in ECG cycle; root-mean-square value of derivative in a single ECG cycle.	*Unitless*
P-Wave Count	PCt	Number of P-waves counted in one sample.	*Count*
P-Wave Height	P-H	Height of P-Wave from isoelectric level.	*mV*
PR-Interval	PR-I	Interval of time between beginning of P-Wave to the beginning of the R-Wave. Can detect atrial conduction block.	*ms*
P-Wave Width	P-Width	Interval of time from the P-Wave to the end of the P-Wave.	*ms*
QaT	QATN	Interval of time between the Q-Wave to the peak of the T-Wave.	*ms*
QR-Interval	QR-I	Interval of time between the Q-Wave to the peak of the R-Wave. Indicator of ventricular depolarization and/or contraction.	*ms*
QRS complex	QRS	Interval of time between the Q-Wave to the beginning of the S-Wave. Indicator of ventricular depolarization and/or contraction.	*ms*
QRS Amplitude	QRSA	Amplitude of QRS complex from the isoelectric level. Indicator of ventricular contraction.	*mV*
QT-Interval	QT-I	Interval of time between the Q-Wave to the end of the T-Wave. Indicator of electrolyte status as well as speed of total cardiac repolarization.	*ms*
R-Wave Height	R-H	Height of the R-Wave from the isoelectric level.	*mV*
RR-Interval	RR-I	Interval from one R-Wave peak to the next R-Wave peak.	*ms*
ST-Elevation	ST-E	Height of the T-Wave at algorithmically-determined point between S-Wave and T-Wave, to detect myocardial infarction.	*mV*
ST-Interval	ST-I	Interval of time between the S-Wave and the end of the T-Wave.	*ms*
T-Wave Height	T-H	Highest point between the end of the S-Wave and end of the T-Wave.	*mV*
Peak of T-Wave	T-P	Peak of T-Wave relative to isoelectric level, between end of S-Wave and end of the T-Wave.	*mV*
T-Wave Peak-to-End	T-Pe	Time between the peak of the T-Wave to the end of the T-Wave; indicator of ventricular reperfusion.	*ms*

Preprints (www.preprints.org) | NOT PEER-REVIEWED | Posted: 11 October 2019 doi:10.20944/preprints201910.0121.v1

Peer-reviewed version available at Pathogens 2019, 8, 240; doi:10.3390/pathogens8040240

References

1. Bennett, J.E.; Dolin, R.; Blaser, M.J. *Mandell, Douglas, and Bennett's principles and practice of infectious diseases*; Elsevier Health Sciences: 2014.
2. Lwande, O.W.; Obanda, V.; Bucht, G.; Mosomtai, G.; Otieno, V.; Ahlm, C.; Evander, M. Global emergence of Alphaviruses that cause arthritis in humans. *Infect Ecol Epidemiol* **2015**, *5*, 29853, doi:10.3402/iee.v5.29853.
3. Weaver, S.C.; Winegar, R.; Manger, I.D.; Forrester, N.L. Alphaviruses: population genetics and determinants of emergence. *Antiviral Res* **2012**, *94*, 242-257, doi:10.1016/j.antiviral.2012.04.002.
4. Greenlee, J.E. The equine encephalitides. *Handb Clin Neurol* **2014**, *123*, 417-432, doi:10.1016/B978-0-444-53488-0.00019-5.
5. Broeck, G.T.; Merrill, M.H. A serological difference between eastern and western equine encephalomyelitis virus. *Proceedings of the Society for Experimental Biology and Medicine* **1933**, *31*, 217-220.
6. Beck, C.E.; Wyckoff, R.W.G. Venezuelan Equine Encephalomyelitis. *Science* **1938**, *88*, 530.
7. Howitt, B.F. Viruses of Equine and of St. Louis Encephalitis in Relationship to Human Infections in California, 1937-1938. *Am J Public Health Nations Health* **1939**, *29*, 1083-1097.
8. Findlay, G. Variation in viruses. In *Handbuch der Virusforschung*, Springer: 1938; pp. 861-994.
9. Hart, B.L.; Ketai, L. Armies of pestilence: CNS infections as potential weapons of mass destruction. *AJNR Am J Neuroradiol* **2015**, *36*, 1018-1025, doi:10.3174/ajnr.A4177.
10. Sidwell, R.W.; Smee, D.F. Viruses of the Bunya- and Togaviridae families: potential as bioterrorism agents and means of control. *Antiviral Res* **2003**, *57*, 101-111.
11. Schmaljohn, A.L.; McClain, D. Alphaviruses (Togaviridae) and Flaviviruses (Flaviviridae). In *Medical Microbiology*, 4th ed.; Baron, S., Ed. Galveston (TX), 1996.
12. Kennedy, P.G. Viral encephalitis: causes, differential diagnosis, and management. *J Neurol Neurosurg Psychiatry* **2004**, *75 Suppl 1*, i10-15.
13. Deresiewicz, R.L.; Thaler, S.J.; Hsu, L.; Zamani, A.A. Clinical and neuroradiographic manifestations of eastern equine encephalitis. *N Engl J Med* **1997**, *336*, 1867-1874, doi:10.1056/NEJM199706263362604.
14. Zacks, M.A.; Paessler, S. Encephalitic alphaviruses. *Vet Microbiol* **2010**, *140*, 281-286, doi:10.1016/j.vetmic.2009.08.023.
15. Delfraro, A.; Burgueno, A.; Morel, N.; Gonzalez, G.; Garcia, A.; Morelli, J.; Perez, W.; Chiparelli, H.; Arbiza, J. Fatal human case of Western equine encephalitis, Uruguay. *Emerg Infect Dis* **2011**, *17*, 952-954, doi:10.3201/eid1705.101068.
16. Gardner, C.L.; Ebel, G.D.; Ryman, K.D.; Klimstra, W.B. Heparan sulfate binding by natural eastern equine encephalitis viruses promotes neurovirulence. *Proc Natl Acad Sci U S A* **2011**, *108*, 16026-16031, doi:10.1073/pnas.1110617108.
17. Pisano, M.B.; Oria, G.; Beskow, G.; Aguilar, J.; Konigheim, B.; Cacace, M.L.; Aguirre, L.; Stein, M.; Contigiani, M.S. Venezuelan equine encephalitis viruses (VEEV) in Argentina: serological evidence of human infection. *PLoS Negl Trop Dis* **2013**, *7*, e2551, doi:10.1371/journal.pntd.0002551.
18. Arechiga-Ceballos, N.; Aguilar-Setien, A. Alphaviral equine encephalomyelitis (Eastern, Western and Venezuelan). *Rev Sci Tech* **2015**, *34*, 491-501.
19. Martin, D.H.; Eddy, G.A.; Sudia, W.D.; Reeves, W.C.; Newhouse, V.F.; Johnson, K.M. An epidemiologic study of Venezuelan equine encephalomyelitis in Costa Rica, 1970. *Am J Epidemiol* **1972**, *95*, 565-578.

Preprints (www.preprints.org) | NOT PEER-REVIEWED | Posted: 11 October 2019 doi:10.20944/preprints201910.0121.v1

Peer-reviewed version available at Pathogens 2019, 8, 240; doi:10.3390/pathogens8040240

20. Rivas, F.; Diaz, L.A.; Cardenas, V.M.; Daza, E.; Bruzon, L.; Alcala, A.; De la Hoz, O.; Caceres, F.M.; Aristizabal, G.; Martinez, J.W., et al. Epidemic Venezuelan equine encephalitis in La Guajira, Colombia, 1995. *J Infect Dis* **1997**, *175*, 828-832.
21. Reeves, W.C. A review of developments associated with the control of Western Equine and St. Louis encephalitis in California during 1967. *Proc Pap Annu Conf Calif Mosq Control Assoc* **1968**, *36*, 65-70.
22. MacKay, J.F.; Stackiw, W.; Brust, R.A. Western encephalitis (W.E.) in Manitoba--1966. *Manit Med Rev* **1968**, *48*, 56-57.
23. Rozdilsky, B.; Robertson, H.E.; Chorney, J. Western encephalitis: report of eight fatal cases. Saskatchewan epidemic, 1965. *Can Med Assoc J* **1968**, *98*, 79-86.
24. Forrester, N.L.; Kenney, J.L.; Deardorff, E.; Wang, E.; Weaver, S.C. Western Equine Encephalitis submergence: lack of evidence for a decline in virus virulence. *Virology* **2008**, *380*, 170-172, doi:10.1016/j.virol.2008.08.012.
25. Przelomski, M.M.; O'Rourke, E.; Grady, G.F.; Berardi, V.P.; Markley, H.G. Eastern equine encephalitis in Massachusetts: a report of 16 cases, 1970-1984. *Neurology* **1988**, *38*, 736-739.
26. Whitley, R.J. Viral encephalitis. *N Engl J Med* **1990**, *323*, 242-250, doi:10.1056/NEJM199007263230406.
27. Wang, E.; Paessler, S.; Aguilar, P.V.; Carrara, A.S.; Ni, H.; Greene, I.P.; Weaver, S.C. Reverse Transcription-PCR-Enzyme-Linked Immunosorbent Assay for Rapid Detection and Differentiation of Alphavirus Infections. *Journal of Clinical Microbiology* **2006**, *44*, 4000-4008, doi:10.1128/jcm.00175-06.
28. Gang Hu, W.; Nagata, L.P. Opportunities and Challenges of Therapeutic Monoclonal Antibodies as Medical Countermeasures for Biodefense. *Journal of Bioterrorism & Biodefense* **2016**, *7*, doi:10.4172/2157-2526.1000149.
29. Burns, D.L. Licensure of vaccines using the Animal Rule. *Current opinion in virology* **2012**, *2*, 353-356.
30. Dupuy, L.C.; Reed, D.S. Nonhuman primate models of encephalitic alphavirus infection: historical review and future perspectives. *Current opinion in virology* **2012**, *2*, 363-367, doi:10.1016/j.coviro.2012.02.014.
31. Pratt, W.D., Fine, D.L., Hart, M.K., Martin, S.S., Reed, D.S. Alphaviruses. In *Biodefense Research Methodology and Animal Models*, 2nd ed.; Swearengen, J.R., Ed. CRC Press: New York, 2012; pp. 223-254.
32. Phillips, A.T.; Rico, A.B.; Stauft, C.B.; Hammond, S.L.; Aboellail, T.A.; Tjalkens, R.B.; Olson, K.E. Entry Sites of Venezuelan and Western Equine Encephalitis Viruses in the Mouse Central Nervous System following Peripheral Infection. *J Virol* **2016**, *90*, 5785-5796, doi:10.1128/JVI.03219-15.
33. Suhrbier, A.; Jaffar-Bandjee, M.C.; Gasque, P. Arthritogenic alphaviruses--an overview. *Nat Rev Rheumatol* **2012**, *8*, 420-429, doi:10.1038/nrrheum.2012.64.
34. Sali, T.M.; Pryke, K.M.; Abraham, J.; Liu, A.; Archer, I.; Broeckel, R.; Staverosky, J.A.; Smith, J.L.; Al-Shammari, A.; Amsler, L., et al. Characterization of a Novel Human-Specific STING Agonist that Elicits Antiviral Activity Against Emerging Alphaviruses. *PLoS Pathog* **2015**, *11*, e1005324, doi:10.1371/journal.ppat.1005324.
35. Reed, Douglas S.; Lind, Cathleen M.; Sullivan, Lawrence J.; Pratt, William D.; Parker, Michael D. Aerosol Infection of Cynomolgus Macaques with Enzootic Strains of Venezuelan Equine Encephalitis Viruses. *The Journal of Infectious Diseases* **2004**, *189*, 1013-1017, doi:10.1086/382281.
36. Reed, Douglas S.; Lackemeyer, Matthew G.; Garza, Nicole L.; Norris, S.; Gamble, S.; Sullivan, Lawrence J.; Lind, Cathleen M.; Raymond, Jo L. Severe Encephalitis in Cynomolgus Macaques Exposed to Aerosolized Eastern Equine Encephalitis Virus. *The Journal of Infectious Diseases* **2007**, *196*, 441-450, doi:10.1086/519391.

Preprints (www.preprints.org) | NOT PEER-REVIEWED | Posted: 11 October 2019 doi:10.20944/preprints201910.0121.v1

Peer-reviewed version available at Pathogens 2019, 8, 240; doi:10.3390/pathogens8040240

37. Chreiteh, S.S.; Fisker, K.B. Morphological Changes of the QRS Complex as a Marker of Autonomic Modulation of the Heart Rate. Aalborg University, Denmark, 2009.
38. Yamaguchi, M.; Shimizu, M.; Ino, H.; Terai, H.; Uchiyama, K.; Oe, K.; Mabuchi, T.; Konno, T.; Kaneda, T.; Mabuchi, H. T wave peak-to-end interval and QT dispersion in acquired long QT syndrome: a new index for arrhythmogenicity. *Clinical Science* **2003**, *105*, 671-676, doi:10.1042/cs20030010.
39. Sztajzel, J. Heart rate variability: a noninvasive electrocardiographic method to measure the autonomic nervous system. *Swiss Med Wkly* **2004**, *134*, 514-522, doi:2004/35/smw-10321.
40. Stein, P.K.; Kleiger, R.E. Insights from the study of heart rate variability. *Annu Rev Med* **1999**, *50*, 249-261, doi:10.1146/annurev.med.50.1.249.
41. Saper, C.B.; Scammell, T.E.; Lu, J. Hypothalamic regulation of sleep and circadian rhythms. *Nature* **2005**, *437*, 1257-1263, doi:10.1038/nature04284.
42. Massin, M.M.; Maeyns, K.; Withofs, N.; Ravet, F.; Gerard, P. Circadian rhythm of heart rate and heart rate variability. *Arch Dis Child* **2000**, *83*, 179-182, doi:10.1136/adc.83.2.179.
43. Carney, R.M.; Blumenthal, J.A.; Freedland, K.E.; Stein, P.K.; Howells, W.B.; Berkman, L.F.; Watkins, L.L.; Czajkowski, S.M.; Hayano, J.; Domitrovich, P.P., et al. Low heart rate variability and the effect of depression on post-myocardial infarction mortality. *Arch Intern Med* **2005**, *165*, 1486-1491, doi:10.1001/archinte.165.13.1486.
44. Singh, J.P.; Larson, M.G.; O'Donnell, C.J.; Wilson, P.F.; Tsuji, H.; Lloyd-Jones, D.M.; Levy, D. Association of hyperglycemia with reduced heart rate variability (The Framingham Heart Study). *Am J Cardiol* **2000**, *86*, 309-312, doi:10.1016/s0002-9149(00)00920-6.
45. Sloan, R.P.; McCreath, H.; Tracey, K.J.; Sidney, S.; Liu, K.; Seeman, T. RR interval variability is inversely related to inflammatory markers: the CARDIA study. *Mol Med* **2007**, *13*, 178-184, doi:10.2119/2006-00112.Sloan.
46. Kleiter, I.; Steinbrecher, A.; Flugel, D.; Bogdahn, U.; Schulte-Mattler, W. Autonomic involvement in tick-borne encephalitis (TBE): report of five cases. *Eur J Med Res* **2006**, *11*, 261-265.
47. La-Orkhun, V.; Supachokchaiwattana, P.; Lertsapcharoen, P.; Khongphatthanayothin, A. Spectrum of cardiac rhythm abnormalities and heart rate variability during the convalescent stage of dengue virus infection: a Holter study. *Ann Trop Paediatr* **2011**, *31*, 123-128, doi:10.1179/1465328111Y.0000000008.
48. Stock, C.; Teyssier, G.; Pichot, V.; Goffaux, P.; Barthelemy, J.C.; Patural, H. Autonomic dysfunction with early respiratory syncytial virus-related infection. *Auton Neurosci* **2010**, *156*, 90-95, doi:10.1016/j.autneu.2010.03.012.
49. Markoff, L. Alphaviruses. In *Mandell, Douglas, and Bennett's Principles and Practice of Infectious Diseases*, Elsevier BV: 2010; 10.1016/b978-0-443-06839-3.00151-xpp 2117-2125.
50. Council, N.R. Guide for the care and use of laboratory animals (National Academy, Washington DC). **1996**.
51. Aebersold, P. FDA experience with medical countermeasures under the animal rule. *Advances in preventive medicine* **2011**, *2012*.
52. Gronvall, G.K.; Trent, D.; Borio, L.; Brey, R.; Nagao, L. The FDA animal efficacy rule and biodefense. *Nature Biotechnology* **2007**, *25*, 1084-1087, doi:10.1038/nbt1007-1084.
53. Wyckoff, R.W.G.; Tesar, W.C. Equine Encephalomyelitis in Monkeys. *The Journal of Immunology* **1939**, *37*, 329-343.
54. Roy, C.; Reed, D.; Hutt, J. Aerobiology and inhalation exposure to biological select agents and toxins. *Veterinary Pathology Online* **2010**, *47*, 779-789.

Preprints (www.preprints.org) | NOT PEER-REVIEWED | Posted: 11 October 2019 doi:10.20944/preprints201910.0121.v1

Peer-reviewed version available at Pathogens 2019, 8, 240; doi:10.3390/pathogens8040240

781 55. Sahin-Yilmaz, A.; Naclerio, R.M. Anatomy and physiology of the upper airway. *Proc Am Thorac Soc* **2011**, *8*, 31-39, doi:10.1513/pats.201007-050RN.
782
783 56. Rossi, S.L.; Russell-Lodrigue, K.E.; Killeen, S.Z.; Wang, E.; Leal, G.; Bergren, N.A.; Vinet-Oliphant, H.; Weaver, S.C.; Roy, C.J. IRES-Containing VEEV Vaccine Protects Cynomolgus Macaques from IE Venezuelan Equine Encephalitis Virus Aerosol Challenge. *PLOS Neglected Tropical Diseases* **2015**, *9*, e0003797, doi:10.1371/journal.pntd.0003797.
784
785
786
787 57. Roy, C.J.; Adams, A.P.; Wang, E.; Leal, G.; Seymour, R.L.; Sivasubramani, S.K.; Mega, W.; Frolov, I.; Didier, P.J.; Weaver, S.C. A chimeric Sindbis-based vaccine protects cynomolgus macaques against a lethal aerosol challenge of eastern equine encephalitis virus. *Vaccine* **2013**, *31*, 1464-1470, doi:10.1016/j.vaccine.2013.01.014.
788
789
790
791 58. Reed, D.S.; Larsen, T.; Sullivan, L.J.; Lind, C.M.; Lackemeyer, M.G.; Pratt, W.D.; Parker, M.D. Aerosol exposure to western equine encephalitis virus causes fever and encephalitis in cynomolgus macaques. *J Infect Dis* **2005**, *192*, 1173-1182, doi:10.1086/444397.
792
793
794 59. Einthoven, W.; Fahr, G.; De Waart, A. On the direction and manifest size of the variations of potential in the human heart and on the influence of the position of the heart on the form of the electrocardiogram. *Am Heart J* **1950**, *40*, 163-211.
795
796
797 60. Gardner, C.L.; Sun, C.; Luke, T.; Raviprakash, K.; Wu, H.; Jiao, J.A.; Sullivan, E.; Reed, D.S.; Ryman, K.D.; Klimstra, W.B. Antibody Preparations from Human Transchromosomic Cows Exhibit Prophylactic and Therapeutic Efficacy against Venezuelan Equine Encephalitis Virus. *J Virol* **2017**, *91*, doi:10.1128/JVI.00226-17.
798
799
800
801 61. Lackemeyer, M.; Kok-Mercado, F.; Wada, J.; Bollinger, L.; Kindrachuk, J.; Wahl-Jensen, V.; Kuhn, J.; Jahrling, P. ABSL-4 Aerobiology Biosafety and Technology at the NIH/NIAID Integrated Research Facility at Fort Detrick. *Viruses* **2014**, *6*, 137-150, doi:10.3390/v6010137.
802
803
804 62. Reed, D.S.; Bethel, L.M.; Powell, D.S.; Caroline, A.L.; Hartman, A.L. Differences in aerosolization of Rift Valley fever virus resulting from choice of inhalation exposure chamber: implications for animal challenge studies. *Pathog Dis* **2014**, *71*, 227-233, doi:10.1111/2049-632X.12157.
805
806
807 63. Bohannon, J.K.; Honko, A.N.; Reeder, R.J.; Cooper, K.; Byrum, R.; Bollinger, L.; Kuhn, J.H.; Wada, J.; Qin, J.; Jahrling, P.B., et al. Comparison of respiratory inductive plethysmography versus head-out plethysmography for anesthetized nonhuman primates in an animal biosafety level 4 facility. *Inhal Toxicol* **2016**, *28*, 670-676, doi:10.1080/08958378.2016.1247199.
808
809
810
811 64. Bowling, J.D.; O'Malley, K.J.; Klimstra, W.B.; Hartman, A.L.; Reed, D.S. A Vibrating Mesh Nebulizer as an Alternative to the Collison Three-Jet Nebulizer for Infectious Disease Aerobiology. *Applied and Environmental Microbiology* **2019**, *85*, e00747-00719, doi:10.1128/AEM.00747-19.
812
813
814 65. Mehendale, A.C.; Doyle, J.M.; Kolin, C.M.; Kroehle, J.P., Jr. Unlock the information in your data: Software to find, classify, and report on data patterns and arrhythmias. *J Pharmacol Toxicol Methods* **2016**, *81*, 99-106, doi:10.1016/j.vascn.2016.05.007.
815
816
817 66. Agnieszka Kitlas, G. Poincaré Plots in Analysis of Selected Biomedical Signals. *Studies in Logic, Grammar and Rhetoric* **2013**, *35*, 117-127, doi:https://doi.org/10.2478/slgr-2013-0031.
818
819 67. Henriques, T.S.; Mariani, S.; Burykin, A.; Rodrigues, F.; Silva, T.F.; Goldberger, A.L. Multiscale Poincaré plots for visualizing the structure of heartbeat time series. *BMC Med Inform Decis Mak* **2016**, *16*, 17-17, doi:10.1186/s12911-016-0252-0.
820
821
822 68. Ma, H. Investigation of the natural history of Equine Encephalitis Viruses with radiofrequency telemetry for detection of subclinical disease patterns. University of Pittsburgh, Pittsburgh (PA), 2017.
823
824